Editors' Suggestion

Laser-stimulated electric quadrupole transitions in the molecular hydrogen ion H_2^+

V. I. Korobov
Bogoliubov Laboratory of Theoretical Physics, Joint Institute for Nuclear Research, 141980 Dubna, Russia

P. Danev and D. Bakalov*
Institute for Nuclear Research and Nuclear Energy, Bulgarian Academy of Sciences, Boulevard Tsarigradsko chausée 72, Sofia 1142, Bulgaria

S. Schiller
Institut für Experimentalphysik, Heinrich-Heine-Universität Düsseldorf, 40225 Düsseldorf, Germany

(Received 16 January 2018; published 12 March 2018)

Molecular hydrogen ions are of metrological relevance due to the possibility of precise theoretical evaluation of their spectrum and of external-field-induced shifts. We report the results of the calculations of the rate of laser-induced electric quadrupole transitions between a large set of ro-vibrational states of H_2^+. The hyperfine and Zeeman structure of the $E2$ transition spectrum and the effects of the laser polarization are treated in detail. The treatment is generally applicable to molecules in $^2\Sigma$ states. We also present the nuclear spin-electron spin-coupling constants, computed with a precision ten times higher than previously obtained.

DOI: 10.1103/PhysRevA.97.032505

I. INTRODUCTION

Molecular hydrogen ions (MHIs) are three-body systems that allow for precise theoretical evaluation of their spectrum and external effect shifts [1,2]. Properly selected transitions exhibit weak sensitivity to external fields. This feature makes them excellent candidates for frequency standards with potential uncertainties at the 10^{-17} fractional level [3,4]. Current and future results from precision spectroscopy of MHIs, combined with the theoretical prediction of transition frequencies, also allows determining several fundamental constants of atomic physics, such as particle mass ratios and the Rydberg constant [5–7].

The spectroscopy of electric quadrupole transitions in homonuclear molecules has been the subject of many investigations, recently in trapped and sympathetically cooled molecular ions (see, e.g., Ref. [8] and references therein). The first theoretical study on the electric quadrupole rovibrational transitions of H_2^+ was published by Bates and Poots in 1953 [9] using the two-center approximation for the wave function. Posen *et al.* [10] computed the spontaneous emission rates for all rovibrational transitions in H_2^+, without inclusion of hyperfine structure. More accurate calculations were performed by Pilon and Baye [11]. Karr [12] treated the hyperfine structure of some $E2$ transitions for the particular case of stretched states.

Recently we [4] and Karr [12] (see also Ref. [3]) pointed out that the electric quadrupole spectroscopy of H_2^+ sympathetically cooled by beryllium ions has outstanding potential for achieving ultrahigh precision. In this context, in Ref. [13] an approach was proposed for quantum-state preparation of H_2^+, which involves laser-driven electric quadrupole transitions.

The strengths of hyperfine-resolved quadrupole transitions for diatomic molecules were recently discussed by Germann and Willitsch [14]. Specifically, they considered Hund's case b_β in J-representation and derived for this particular case general expressions for the line strength in zeroth order of perturbation theory in the spin interactions without taking into account the dependence on laser polarization.

In this work, we present a complete treatment of the electric quadrupole transitions of H_2^+, including both the spin (hyperfine) structure and the effects of magnetic field and laser polarization. Similar to the extensive work in Ref. [10] we have considered transitions between higher excited states with vibration quantum number up to $v = 10$.

In the following, we derive the explicit expressions for the interaction of a monochromatic wave with the H_2^+ molecule in an arbitrary quantum state, starting with the basics in Sec. II A. The hyperfine structure of the levels of H_2^+ is introduced in Sec. II B, followed by the computation of the energies of the spin states. High accuracy was made possible by an improved computation of the spin-spin coupling coefficients. A detailed treatment of the transition strengths of the spin components of a given rovibrational transition is worked out in Sec. II C. We pay particular attention to making our results easily comparable with previous work. Section III is devoted to the discussion of some examples that are believed to be of relevance for near-future precision spectroscopic studies.

II. THEORY

A. Interaction with an external electromagnetic field

In the center-of-mass frame, the nonrelativistic Hamiltonian of H_2^+ is

$$H^{\rm NR} = \frac{\mathbf{P}_1^2}{2m_p} + \frac{\mathbf{P}_2^2}{2m_p} + \frac{\mathbf{P}_e^2}{2m_e} + \frac{e^2}{4\pi\varepsilon_0}\left(-\frac{1}{r_1} - \frac{1}{r_2} + \frac{1}{r_{12}}\right), \tag{1}$$

*bakal10@abv.bg

where $\mathbf{R}_{1,2}$, $\mathbf{R}_e$ and $\mathbf{P}_{1,2}$, $\mathbf{P}_e$ are the position and momentum operators of the two protons and the electron, respectively; $\mathbf{r}_1 = \mathbf{R}_e - \mathbf{R}_1$, $\mathbf{r}_2 = \mathbf{R}_e - \mathbf{R}_2$, $\mathbf{r}_{12} = \mathbf{R}_1 - \mathbf{R}_2$, and m_p and m_e are the masses of the proton and the electron, respectively.

The interaction Hamiltonian of a system of particles with an external electromagnetic field is [15]

$$H_{\rm int} = -\sum_\alpha \frac{Z_\alpha e}{m_\alpha} \mathbf{P}_\alpha \cdot \mathbf{A}(\mathbf{R}_\alpha, t). \tag{2}$$

In Eq. (2) we have kept only the linear terms in the vector potential $\mathbf{A}(\mathbf{R},t)$; e is the magnitude of the electron charge, the summation runs over all three constituents of H_2^+ ($\alpha = p_1, p_2, e^-$), and Z_α is the charge of particle α in units of e. For a plane wave with general polarization the electromagnetic vector potential is

$$\mathbf{A}(\mathbf{R},t) = \mathbf{A}_0 e^{i(\mathbf{k}\cdot\mathbf{R}-\omega t)} + \mathbf{A}_0^* e^{-i(\mathbf{k}\cdot\mathbf{R}-\omega t)}$$

and corresponds to the electric field

$$\mathbf{E}(\mathbf{R},t) = \mathbf{E}_0 e^{i(\mathbf{k}\cdot\mathbf{R}-\omega t)} + \mathbf{E}_0^* e^{-i(\mathbf{k}\cdot\mathbf{R}-\omega t)}, \quad \mathbf{E}_0 = i\omega \mathbf{A}_0. \tag{3}$$

$\mathbf{A}_0$ is a complex vector satisfying $\mathbf{A}_0 \cdot \mathbf{k} = 0$. In the long-wavelength approximation, we expand the exponent $e^{\pm i(\mathbf{k}\cdot\mathbf{R}_\alpha)}$ in Eq. (2) and keep only the terms responsible for the electric quadrupole transitions:

$$H_{\rm int}^{(2)} = -\sum_\alpha \frac{Z_\alpha e}{m_\alpha} \mathbf{P}_\alpha \cdot (i\mathbf{A}_0 e^{-i\omega t}(\mathbf{k}\cdot\mathbf{R}_\alpha) + \text{c.c.}). \tag{4}$$

The above expression can be rewritten as a sum of terms, each of which is the product of two either symmetric or antisymmetric tensors. The product of antisymmetric tensors gives rise to magnetic dipole transitions and is not considered here. The remaining terms are put in the form [15]

$$H_{\rm int}^{(E2)} = \frac{i}{\hbar} \sum_\alpha \frac{Z_\alpha e}{2\omega} \sum_{ij} T_{ij}^{(2)}(t)[R_{\alpha i} R_{\alpha j}, H^{\rm NR}]. \tag{5}$$

Here $T_{ij}^{(2)}(t) = \frac{1}{2}(k_i E_j(0,t) + k_j E_i(0,t))$ is the symmetric part of the tensor product of the electric field at the center of mass of the system, $\mathbf{E}(0,t)$, and of the wave vector, $\mathbf{k}$. We also make use of the dimensionless, time-independent, and complex tensor

$$\widehat{T}_{ij}^{(2)} = (\hat{k}_i \hat{\epsilon}_j + \hat{k}_j \hat{\epsilon}_i)/2, \tag{6}$$

where $\hat{k}$ and $\hat{\epsilon}$ are unit vectors along $\mathbf{k}$ and $\mathbf{E}_0$: $\mathbf{k} = k\hat{\mathbf{k}}$ $= (\omega/c)\hat{\mathbf{k}}$, $\mathbf{E}_0 = |\mathbf{E}_0|\,\hat{\epsilon}$. The relation of $T_{ij}^{(2)}(t)$ to $\widehat{T}_{ij}^{(2)}$ reads

$$T_{ij}^{(2)}(t) = k|\mathbf{E}_0|\big(\widehat{T}_{ij}^{(2)}\, e^{-i\omega t} + \widehat{T}_{ij}^{(2)*}\, e^{i\omega t}\big). \tag{7}$$

B. H_2^+ hyperfine structure

The calculations in this work are done in the total angular momentum representation with the following coupling scheme of angular momentum operators:

$$\mathbf{I} = \mathbf{I}_1 + \mathbf{I}_2, \qquad \mathbf{F} = \mathbf{I} + \mathbf{s}_e, \qquad \mathbf{J} = \mathbf{L} + \mathbf{F}. \tag{8}$$

$\mathbf{I}_{1,2}$ and $\mathbf{s}_e$ are the spin operators of the two protons and electron, respectively, $\mathbf{L}$ is the total orbital momentum, and $\mathbf{J}$ is the total angular momentum.

The H_2^+ molecular ion has a simple hyperfine structure. As a homonuclear molecule with fermionic nuclei, its state vectors are antisymmetric with respect to the exchange of the protons. This property gives rise to a restriction on the total nuclear spin quantum number $(-1)^I = (-1)^L$ (for the ground electronic state $1s\sigma_g$), which therefore becomes an exact quantum number [16]. The other exact quantum numbers are J and the z-axis projection J_z. Although F is not conserved, it can be used as a label of the hyperfine states since the mixing in F is small (see the table in the Supplemental Material [17]). The states with odd orbital quantum number L are split into six hyperfine components, $(F,J) = (1/2, L \pm 1/2)$, $(3/2, L \pm 1/2)$, $(3/2, L \pm 3/2)$, and for even L into two components, $(F,J) = (1/2, L \pm 1/2)$. Exceptions are the $L = 0$ state with a single component $(F,J) = (1/2, L + 1/2)$, and $L = 1$, which has five components: $(F,J) = (1/2, L \pm 1/2)$, $(3/2, L \pm 1/2)$, $(3/2, L + 3/2)$.

The hyperfine energies $E_{(vL)FJ}^{\rm hfs}$ and state vectors are calculated by diagonalization of the effective state-dependent spin Hamiltonian $H^{\rm eff}$, obtained from the Breit-Pauli interaction by averaging over space variables with the nonrelativistic wave functions of H_2^+ [18,19]:

$$\begin{aligned} H^{\rm eff} = {} & b_f(\mathbf{I}\cdot\mathbf{s}_e) + c_e(\mathbf{L}\cdot\mathbf{s}_e) + c_I(\mathbf{L}\cdot\mathbf{I}) + \frac{d_1}{(2L-1)(2L+3)} \\ & \times \left(\frac{2}{3}\mathbf{L}^2(\mathbf{I}\cdot\mathbf{s}_e) - [(\mathbf{L}\cdot\mathbf{I})(\mathbf{L}\cdot\mathbf{s}_e) + (\mathbf{L}\cdot\mathbf{s}_e)(\mathbf{L}\cdot\mathbf{I})]\right) \\ & + \frac{d_2}{(2L-1)(2L+3)}\left(\frac{1}{3}\mathbf{L}^2\mathbf{I}^2 - \frac{1}{2}(\mathbf{L}\cdot\mathbf{I}) - (\mathbf{L}\cdot\mathbf{I})^2\right). \end{aligned} \tag{9}$$

The state-dependent coefficients b_f, c_e, c_I, d_1, and d_2 are calculated numerically. In this paper we use the recently updated values of b_f, in which the contributions of order $O(m_e\alpha^6)$, amounting to 10^{-4} fractionally, have been accounted for. For the remaining coefficients we use the values calculated in Ref. [18]. The magnitude of the coefficient b_f dominates over the others, which justifies the choice of angular momentum coupling given in Eq. (8) rather than Hund's case (b). $H^{\rm eff}$ is an operator acting in the space of spin variables and total orbital angular momentum L, which is spanned by the basis vectors

$$\begin{aligned} |LIFJJ_z\rangle = {} & \sum_{\zeta_1\zeta_2 I_z \zeta_e F_z L_z} C^{II_z}_{I_1\zeta_1, I_2\zeta_2} C^{FF_z}_{II_z, s_e\zeta_e} C^{JJ_z}_{FF_z, LL_z} \\ & \times |I_1\zeta_1\rangle |I_2\zeta_2\rangle |s_e\zeta_e\rangle |LL_z\rangle. \end{aligned} \tag{10}$$

Here $|LL_z\rangle$ satisfies $(\mathbf{L}^2 - L(L+1))|LL_z\rangle = 0$, $(\mathbf{L}_z - L_z)|LL_z\rangle = 0$, and similar for the individual particle spin operators and eigenvectors, and C are Clebsch-Gordan coefficients. In first-order perturbation theory the hyperfine state vectors, $|(vL)FJJ_z\rangle$, are expressed as linear combinations of the basis vectors $|LIFJJ_z\rangle$:

$$|(vL)FJJ_z\rangle = \sum_{F'} \beta_{F'}^{(vL)FJ} |LIF'JJ_z\rangle, \tag{11}$$

where $\beta_{F'}^{(vL)FJ}$ are the components of the eigenvectors of the matrix of $H^{\rm eff}$ in the basis (10), and the values of F' satisfy the inequalities $\max(|I-1/2|, |J-L|) \leqslant F' \leqslant \min(I+1/2, J+L)$. In the absence of external fields, the

TABLE I. Hyperfine structure of the lower rovibrational states of H_2^+ with orbital momentum L in the range $0 \leqslant L \leqslant 4$ and vibrational quantum number v in the range $0 \leqslant v \leqslant 8$. Listed are the updated values (in MHz) of the coefficient b_f in the effective spin Hamiltonian $H^{\rm eff}$ [Eq. (9)], the hyperfine energies $E^{\rm hfs}_{(vL)FJ}$ (in MHz), and, for odd L, the mixing angles $\phi_\pm$ (in rad). In parentheses are given the quantum numbers (F, J).

		b_f (MHz)	$E^{\rm hfs}_{(vL)FJ}$ (MHz)						Mixing angles				$E^{\rm hfs}_{(vL)FJ}$ (MHz)	
L	v		$(\frac{3}{2},L+\frac{3}{2})$	$(\frac{3}{2},L+\frac{1}{2})$	$(\frac{1}{2},L+\frac{1}{2})$	$(\frac{3}{2},L-\frac{1}{2})$	$(\frac{1}{2},L-\frac{1}{2})$	$(\frac{3}{2},L-\frac{3}{2})$	ϕ_+	ϕ_-	L	v	$(\frac{1}{2},L+\frac{1}{2})$	$(\frac{1}{2},L-\frac{1}{2})$
1	0	922.9318	474.0763	481.9234	−930.3732	385.3687	−910.6980		−0.01561	−0.03890	2	0	42.1625	−63.2438
1	1	898.7507	461.2282	468.4956	−905.7253	377.9657	−887.1909		−0.01508	−0.03736	2	1	39.5716	−59.3574
1	2	876.3973	449.3273	456.0493	−882.9269	371.2588	−865.4856		−0.01452	−0.03578	2	2	37.0992	−55.6487
1	3	855.7571	438.3119	444.5191	−861.8606	365.2188	−845.4716		−0.01395	−0.03417	2	3	34.7295	−52.0943
1	4	836.7296	428.1272	433.8475	−842.4234	359.8226	−827.0524		−0.01335	−0.03253	2	4	32.4479	−48.6718
1	5	819.2274	418.7256	423.9833	−824.5255	355.0518	−810.1443		−0.01273	−0.03084	2	5	30.2400	−45.3600
1	6	803.1750	410.0651	414.8819	−808.0888	350.8940	−794.6756		−0.01209	−0.02911	4	0	82.5884	−103.2355
1	7	788.5079	402.1094	406.5042	−793.0463	347.3416	−780.5856		−0.01142	−0.02733	4	1	77.4966	−96.8707
1	8	775.1714	394.8271	398.8163	−779.3412	344.3925	−767.8240		−0.01071	−0.02548	4	2	72.6350	−90.7937
3	0	917.5313	507.2270	489.4960	−941.0438	423.6046	−894.6020	341.5241	−0.04213	−0.06186	4	3	67.9728	−84.9660
3	1	893.6964	492.3526	475.5481	−915.6828	413.6522	−871.9908	336.8955	−0.04067	−0.05948	4	4	63.4807	−79.3509
3	2	871.6711	478.5158	462.6063	−892.2046	404.5273	−851.1450	332.8336	−0.03916	−0.05705				
3	3	851.3432	465.6422	450.6022	−870.4878	396.1856	−831.9595	329.3264	−0.03761	−0.05456				
3	4	832.6144	453.6659	439.4752	−850.4255	388.5894	−814.3434	326.3667	−0.03599	−0.05200				
3	5	815.3996	442.5281	429.1720	−831.9247	381.7075	−798.2185	323.9516	−0.03432	−0.04937				
3	6	799.6258	432.1751	419.6456	−814.9040	375.5153	−783.5195	322.0852	−0.03257	−0.04664				
3	7	785.2282	422.5607	410.8538	−799.2920	369.9910	−770.1888	320.7713	−0.03074	−0.04382				
3	8	772.1561	413.6433	402.7612	−785.0303	365.1210	−758.1833	320.0235	−0.02882	−0.04090				

energy levels are degenerate in J_z. The nonzero components $\beta_{F'}^{(vL)FJ}$ can be parametrized as follows: for odd L ($I = 1$), $\beta_{3/2}^{(vL)3/2L\pm3/2} = 1$, $\beta_F^{(vL)FL\pm1/2} = \cos\phi_\pm$, $F = 1/2,3/2$, $\beta_{3/2}^{(vL)1/2L\pm1/2} = -\beta_{1/2}^{(vL)3/2L\pm1/2} = \sin\phi_\pm$; for even values of L ($I = 0$), $\beta_{1/2}^{(vL)1/2,L\pm1/2} = 1$, $\beta_{3/2}^{(vL)1/2,L\pm1/2} = 0$. The energies $E^{\rm hfs}_{(vL)FJ}$, the mixing angles $\phi_\pm$ between spin basis states, and the coefficients b_f are given in Table I for vibrational and rotational quantum numbers in the ranges $0 \leqslant v \leqslant 4$ and $0 \leqslant L \leqslant 8$. The small values of the mixing angles confirm the appropriateness of the coupling scheme in Eq. (8) for the classification of the hyperfine structure of the rovibrational spectrum of H_2^+ and justify the use—in lower-accuracy estimates—of the zero-order approximation for the hyperfine state vectors, which reads

$$\phi_\pm \approx 0, \quad \beta_{F'}^{(vL)FJ} \approx \delta_{FF'}. \tag{12}$$

C. *E*2 transition matrix elements and transition rates

Using Eqs. (5) and (7), the $E2$ transition matrix element between initial $|i\rangle = |(vL)FJJ_z\rangle$ and final $|f\rangle = |(v'L')F'J'J'_z\rangle$ hyperfine states of H_2^+ can be put in a form that exhibits the dependence on time:

$$\begin{aligned}
&\langle(v'L')F'J'J'_z\big|H^{(E2)}_{\rm int}\big|(vL)FJJ_z\rangle \\
&= \frac{i}{3}\frac{\omega^{\rm NR}}{\omega}\,\langle(v'L')F'J'J'_z|T^{(2)}(t)\cdot Q^{(2)}|(vL)FJJ_z\rangle \\
&= \frac{i}{3c}\omega^{\rm NR}\,|\mathbf{E}_0|\big(e^{-i\omega t}\langle(v'L')F'J'J'_z|\widehat{T}^{(2)}\cdot Q^{(2)}|(vL)FJJ_z\rangle \\
&\quad + e^{i\omega t}\langle(v'L')F'J'J'_z|\widehat{T}^{(2)*}\cdot Q^{(2)}|(vL)FJJ_z\rangle\big).
\end{aligned} \tag{13}$$

Here $\omega^{\rm NR} = (E^{\rm NR}_{v'L'} - E^{\rm NR}_{vL})/\hbar$, $E^{\rm NR}_{vL}$ and $E^{\rm NR}_{v'L'}$ are the nonrelativistic energies of the initial and final states, $Q^{(2)}$ is the irreducible tensor of the electric quadrupole moment of H_2^+,

$$Q_{ij} = \frac{3}{2}\sum_\alpha Z_\alpha e\left(R_{i\alpha}R_{j\alpha} - \frac{1}{3}(\mathbf{R}_\alpha)^2\delta_{ij}\right), \tag{14}$$

and $T^{(2)}(t)\cdot Q^{(2)} \equiv \sum_{ij} T^{(2)}_{ij}(t)Q^{(2)}_{ij}$ denotes the scalar product of the tensors. The cyclic components $Q^{(2)}_q$ and $T^{(2)q}(t)$, $q = -2,\ldots,2$, are normalized by $Q^{(2)}_0 = Q_{zz}$ and similarly for $T^{(2)0}$ (cf. Refs. [12,20]). In terms of the cyclic components the scalar product is expressed as $T^{(2)}\cdot Q^{(2)} = \frac{3}{2}\sum_q T^{(2)q}(t)Q^{(2)}_q$. Some authors use alternative normalization conventions (e.g., Refs. [21,22]); the current convention was selected to ease comparison with the numerical results of Refs. [11,12]. In these notations the Rabi frequency of the $|(vL)FJJ_z\rangle \to |(v'L')F'J'J'_z\rangle$ transition is given by [20]

$$\Omega_{if} = \frac{|\mathbf{E}_0|\,\omega_{if}}{3\hbar c}|\langle(v'L')F'J'J'_z|\,\widehat{T}^{(2)}\cdot Q^{(2)}\,|(vL)FJJ_z\rangle|. \tag{15}$$

Next, using Eq. (11), for the time-independent matrix elements of $\widehat{T}^{(2)}\cdot Q^{(2)}$ we have

$$\begin{aligned}
&\langle(v'L')F'J'J'_z|\widehat{T}^{(2)}\cdot Q^{(2)}|(vL)FJJ_z\rangle \\
&= \frac{3}{2}\sum_q \widehat{T}^{(2)q}\sum_{F_1,F'_1}\beta_{F_1}^{(vL)FJ}\,\beta_{F'_1}^{(v'L')F'J'}\langle L'IF'_1J'J'_z|Q^{(2)}_1|LIF_1JJ_z\rangle.
\end{aligned} \tag{16}$$

Using the Wigner-Eckart theorem the matrix elements of $Q^{(2)}$ in the basis set (10) are expressed in terms of the nonrelativistic

reduced matrix elements $\langle v'L'\|Q^{(2)}\|vL\rangle$:

$$\langle L'IF_1'J'J_z'|Q_q^{(2)}|LIF_1JJ_z\rangle = \delta_{F_1'F_1}(-1)^{J+L+F_1}\sqrt{2J+1}\,C^{J'J_z'}_{JJ_z,2q} \times \begin{Bmatrix} L & F_1 & J \\ J' & 2 & L' \end{Bmatrix}\langle v'L'\|Q^{(2)}\|vL\rangle.$$

The above expression implies the selection rules $\Delta L \equiv L' - L = 0, \pm 2$, $|\Delta J| \leqslant 2$, and $J + J' \geqslant 2$; the transitions $L = 0 \to L' = 0$ are also forbidden.

The probability $\mathcal{W}_{if}(T)$ for a particular $E2$ transition $|i\rangle \to |f\rangle$ in the time interval $0 \leqslant t \leqslant T$, $\omega T \gg 1$, stimulated by the external electromagnetic field $\mathbf{E}$ oscillating with frequency ω, is [15]

$$\mathcal{W}_{if}(T) = \left|\frac{1}{\hbar}\int_0^T dt\, \exp(i\omega_{if}t)\,\langle (v'L')F'J'J_z'|H_{\rm int}^{(E2)}|(vL)FJJ_z\rangle\right|^2 \approx \Omega_{if}^2(F(\omega-\omega_{if};T) + F(\omega+\omega_{if};T)), \quad (17)$$

where $\omega_{if} = (E_f - E_i)/\hbar$ is the transition angular frequency with account of the hyperfine, Zeeman, etc., corrections to $\omega^{\rm NR}$, and the following δ-like function is used: $F(a;T) = (\sin(aT/2)/(a/2))^2$, $\lim_{T\to\infty} F(a;T) = 2\pi T\delta(a)$. The rate $\mathcal{W}_{if}$ of the transition is defined as the probability per unit time over a sufficiently long time interval: $\mathcal{W}_{if} = \mathcal{W}_{if}(T)/T$, $\omega T \gg 1$. We put the expression of $\mathcal{W}_{if}$ in a form that accounts for the characteristics of the laser source and the transition line profile and distinctly exhibits the hyperfine and Zeeman structure of the spectrum. To this end we relate the amplitude $\mathbf{E}_0$ of the electric field to the spectral density of the laser energy flux $\mathcal{I}(\omega)$: $\mathcal{I}(\omega) = (\varepsilon_0 c/2)\,(d|\mathbf{E}_0|^2/d\omega)$, normalized to the laser intensity $\mathcal{I}_0$ by $\int d\omega\,\mathcal{I}(\omega) = \mathcal{I}_0$. We also denote by $g_{if}(\omega)$ the transition line spectral profile (determined by Doppler broadening or other), with normalization $\int d\omega\, g_{if}(\omega) = 1$. By combining Eqs. (13)–(17), in the limit of large T, the expression for $\mathcal{W}_{if}$ is cast in the following factorized form:

$$\mathcal{W}_{if} = \mathcal{W}^{\rm NR}(v'L';vL)\mathcal{W}^{\rm hfs}((v'L')F'J';(vL)FJ) \times \mathcal{W}^{\rm pol}(J_z';J_z). \quad (18)$$

The first factor, $\mathcal{W}^{\rm NR}(v'L';vL)$, is the rate of stimulated $E2$ transitions in H_2^+ in the nonrelativistic (spinless) approximation, averaged over the initial and summed over the final angular momentum projections J_z, J_z',

$$\mathcal{W}^{\rm NR}(v'L';vL) = \frac{\pi\omega_{if}^2}{\varepsilon_0 c^3\hbar^2}\frac{1}{15(2L+1)}|\langle v'L'||Q^{(2)}||vL\rangle|^2\,\bar{\mathcal{I}}, \qquad \bar{\mathcal{I}} = \int d\omega\,\mathcal{I}(\omega)g_{if}(\omega). \quad (19)$$

The factor $\mathcal{W}^{\rm hfs}((v'L')F'J';(vL)FJ)$ is the relative intensity of the individual hyperfine components $FJ \to F'J'$ of the transition line $(vL) \to (v'L')$. For simplicity of notation we omit v, L, v', and L' wherever possible:

$$\mathcal{W}^{\rm hfs}((v'L')F'J';(vL)FJ) \equiv \mathcal{W}^{\rm hfs}(F'J';FJ) = (2L+1)(2J+1)(2J'+1) \times \left(\sum_{F_1}\beta_{F_1}^{(v'L')F'J'}\beta_{F_1}^{(vL)FJ}(-1)^{J+F_1}\begin{Bmatrix} L & F_1 & J \\ J' & 2 & L' \end{Bmatrix}\right)^2. \quad (20)$$

It is normalized by the condition

$$\sum_{F'J'}\frac{1}{n^{\rm hfs}(vL)}\sum_{FJ}\mathcal{W}^{\rm hfs}(F'J';FJ) = 1, \quad (21)$$

where $n^{\rm hfs}(vL) = 2(2I+1)(2L+1)$ stands for the number of states $|(vL)FJJ_z\rangle$ of the hyperfine structure of the initial rovibrational (vL) state. Note that the approximate expression for $\mathcal{W}^{\rm hfs}(F'J';FJ)$ that stems from the approximation for the amplitudes $\beta_{F'}^{(vL)FJ}$ of zero-order perturbation theory in Eq. (12),

$$\mathcal{W}^{\rm hfs}(F'J';FJ) \approx \delta_{FF'}(2L+1)(2J+1)(2J'+1) \times \begin{Bmatrix} L & F & J \\ J' & 2 & L' \end{Bmatrix}^2, \quad (22)$$

does not describe the "weak" hyperfine components of the transition lines.

Finally, $\mathcal{W}^{\rm pol}(J_z', J_z)$ is the relative intensity of the Zeeman components of the transition line with different values of the quantum numbers J_z, J_z' (the dependence on J and J' being omitted for simplicity of notation):

$$\mathcal{W}^{\rm pol}(J_z';J_z) = \frac{15}{2J'+1}\left(C^{J'J_z'}_{JJ_z,2q}\right)^2|\widehat{T}^{(2)q}|^2, \quad q = J_z' - J_z. \quad (23)$$

$\mathcal{W}^{\rm pol}(J_z';J_z)$ is expressed in terms of Clebsch-Gordan coefficients and of the tensor $\widehat{T}^{(2)}$ defined in Eq. (6), and satisfies

$$\sum_{J_z,J_z'}\mathcal{W}^{\rm pol}(J_z',J_z) = 1. \quad (24)$$

To avoid any ambiguity, we list the general expressions of $\widehat{T}^{(2)q}$ in terms of the Cartesian components of $\hat{\mathbf{k}}$ and $\hat{\epsilon}$:

$$\widehat{T}^{(2)\pm2} = \sqrt{\frac{3}{8}}(\hat{k}_x\hat{\epsilon}_x - \hat{k}_y\hat{\epsilon}_y \mp i(\hat{k}_x\hat{\epsilon}_y + \hat{k}_y\hat{\epsilon}_x)),$$
$$\widehat{T}^{(2)\pm1} = \sqrt{\frac{3}{8}}(\mp(\hat{k}_x\hat{\epsilon}_z + \hat{k}_z\hat{\epsilon}_x) + i(\hat{k}_z\hat{\epsilon}_y + \hat{k}_y\hat{\epsilon}_z)),$$
$$\widehat{T}^{(2)0} = \frac{1}{2}(2\hat{k}_z\hat{\epsilon}_z - \hat{k}_x\hat{\epsilon}_x - \hat{k}_y\hat{\epsilon}_y).$$

The relevance of each of the three factors in Eq. (18) is discussed below.

III. NUMERICAL RESULTS AND DISCUSSION

A. $E2$ transition rates in the approximation of spinless particles

The computational challenge in the present paper was the evaluation of the reduced matrix elements of the electric quadrupole moment of H_2^+ in Eq. (19). The values of $\langle v'L'||Q^{(2)}||vL\rangle$ were calculated with the variational wave functions obtained in the approach of Ref. [23].

TABLE II. Numerical results for selected $E2$ transitions in H_2^+ in the approximation of spinless particles. Comparison with the values of Einstein coefficients A, calculated by Pilon and Baye [11], and of the reduced matrix elements $\langle v'L'||Q^{(2)}||vL\rangle$ of Karr [12] is made in a few illustrative cases considered by those authors. The notation $a[b] = a \times 10^b$ has been used.

i f		$\lvert\langle v'L'\rVert Q^{(2)}\rVert vL\rangle\rvert/ea_0^2$		Einstein coefficient A_{fi} (s^{-1})	
$\lvert vL\rangle \to \lvert v',L'\rangle$	$\Delta E^{\rm NR}/hc$ (cm^{-1})	This work	Karr [12]	This work	Pilon and Baye [11]
$\lvert 0,0\rangle \to \lvert 0,2\rangle$	174.230	1.644960		0.973137[−11]	0.973137[−11]
$\lvert 0,0\rangle \to \lvert 1,2\rangle$	2356.155	0.313846		0.160207[−6]	0.160207[−6]
$\lvert 0,0\rangle \to \lvert 4,2\rangle$	8156.599	0.001048		0.888671[−9]	
$\lvert 0,0\rangle \to \lvert 6,2\rangle$	11436.092	0.000100		0.441771[−10]	
$\lvert 0,1\rangle \to \lvert 1,1\rangle$	2188.035	0.376163	0.3762	0.264911[−6]	0.264911[−6]
$\lvert 0,1\rangle \to \lvert 2,1\rangle$	4248.965	0.028875	0.02887	0.431045[−7]	0.431045[−7]
$\lvert 0,1\rangle \to \lvert 3,1\rangle$	6186.996	0.004044	0.004044	0.553479[−8]	0.553479[−8]
$\lvert 0,1\rangle \to \lvert 4,1\rangle$	8005.682	0.000792		0.770296[−9]	
$\lvert 0,2\rangle \to \lvert 1,2\rangle$	2181.925	0.411812	0.4118	0.185876[−6]	0.185876[−6]
$\lvert 0,2\rangle \to \lvert 2,2\rangle$	4236.951	0.031686	0.03169	0.307072[−7]	0.307072[−7]
$\lvert 0,2\rangle \to \lvert 4,2\rangle$	7982.369	0.000874		0.554230[−9]	
$\lvert 0,3\rangle \to \lvert 1,1\rangle$	1899.184	0.529496	0.5295	0.258605[−6]	0.258605[−6]
$\lvert 0,4\rangle \to \lvert 1,2\rangle$	1780.716	0.667785	0.6678	0.178844[−6]	0.178844[−6]
$\lvert 0,4\rangle \to \lvert 2,4\rangle$	4195.295	0.041347		0.276482[−7]	0.276482[−7]
$\lvert 0,4\rangle \to \lvert 3,2\rangle$	5768.052	0.002013	0.002013	0.579405[−9]	0.579407[−9]
$\lvert 0,6\rangle \to \lvert 5,6\rangle$	9425.184	0.000367		0.864640[−10]	
$\lvert 1,1\rangle \to \lvert 1,3\rangle$	273.621	2.529827		0.157047[−9]	0.157047[−9]
$\lvert 1,1\rangle \to \lvert 3,3\rangle$	4243.606	0.074474		0.122120[−6]	0.122120[−6]
$\lvert 2,0\rangle \to \lvert 4,2\rangle$	3901.609	0.080164		0.130139[−6]	
$\lvert 3,2\rangle \to \lvert 6,4\rangle$	5375.331	0.049248		0.135446[−6]	
$\lvert 5,2\rangle \to \lvert 5,4\rangle$	301.389	4.850333		0.728017[−9]	
$\lvert 4,3\rangle \to \lvert 10,5\rangle$	8708.227	0.006665		0.226499[−7]	
$\lvert 9,6\rangle \to \lvert 10,6\rangle$	1087.942	3.085308		0.124992[−6]	

Some authors present the rates of transitions in terms of the Einstein coefficients A_{fi} rather than $\mathcal{W}_{if}$, related to the reduced matrix elements by [11]

$$A_{fi}/t_0^{-1} = \frac{\alpha^5}{15(2L+1)}\left(\left(E^{\rm NR}_{v'L'} - E^{\rm NR}_{vL}\right)/\mathcal{E}_0\right)^5 \times \left(\langle v'L'||Q^{(2)}||vL\rangle/\left(ea_0^2\right)\right)^2, \quad (25)$$

where a_0, $t_0 = a_0/\alpha c$, and $\mathcal{E}_0 = 2\mathrm{Ry}$ are the atomic units of length (i.e., the Bohr radius), time, and energy. The numerical results, including the nonrelativistic $E2$ transition frequencies, the values of the reduced matrix elements and of Einstein coefficients for *all* $E2$ transitions between states with vibrational quantum number $0 \leqslant v \leqslant 10$, $|v' - v| \leqslant 6$, and total orbital momentum $0 \leqslant L \leqslant 6$ are given in the table of the Supplemental Material [17]. The considered transitions belong to the near- and mid-infrared spectral range; they are to some extent complementary to the set of states considered in previous works [11,12] and include higher vibrational excitations. The results are intended to help select transitions of appropriate wavelength and intensity and plan future experiments on $E2$ spectroscopy of H_2^+.

Table II illustrates via a few examples the agreement between the numerical values of the reduced matrix elements of the H_2^+ electric quadrupole moment calculated in Refs. [11,12] and in the present work. In the overlapping cases the numerical results agree within the claimed precision of six digits with exceptions that should be attributed to the different ways of rounding.

B. Hyperfine structure of the $E2$ transition spectrum

The approximation of spinless particles, in which the $E2$ transition spectral lines are labeled with the quantum numbers (v, L) and (v', L') of the initial and final states of H_2^+, is applicable only if the spectroscopic resolution is $\simeq$1 GHz or worse. Under higher resolution, every line will evidence splitting into a set of hyperfine components spread over an interval of the order of 1 GHz around the central transition frequency of the hyperfine manifold ω_0 (see Fig. 1). The difference between $\omega^{\rm NR}$ and ω_0 is due to the spin-independent relativistic and QED effects that shift the manifold as a whole. Transitions having $\Delta F \equiv F' - F = \pm 1$ are strongly suppressed compared with transitions with $\Delta F = 0$; the latter are spread over a much narrower frequency interval of the order of 100 MHz. In the assumption of a flat laser spectral profile $\mathcal{I}(\omega)$ the sum of the transition rates (also referred to as line intensities) of all the hyperfine lines equals the nonrelativistic intensity $\mathcal{W}^{\rm NR}(v'L'; vL)$, Eq. (19). The relative intensity of the hyperfine components is given by the factor $\mathcal{W}^{\rm hfs}$ in Eqs. (18) and (20).

Table III lists the energy shift $\Delta E^{\rm hfs}$ and relative intensity $\mathcal{W}^{\rm hfs}(F'J'; FJ)$ of the strong components of a few $E2$ transitions of interest for precision spectroscopy. Note the much simpler structure of the hyperfine spectrum between levels with even L.

C. Laser polarization effects

If the Zeeman structure is not resolved, for example, when the magnetic field strength is small or the Doppler broadening

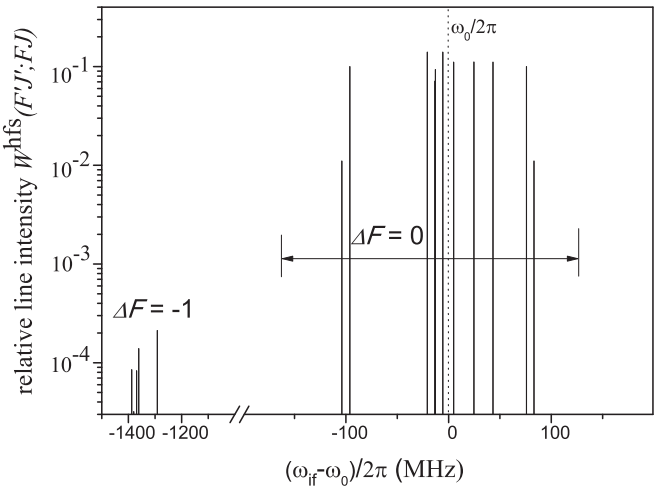

FIG. 1. Hyperfine structure of the $(0,1) \to (1,1)$ $E2$ transition line: relative intensity $\mathcal{W}^{\rm hfs}(F'J';FJ)$ of the individual hyperfine components $(FJ) \to (F'J')$, calculated using Eq. (20). The "weak" components with $\Delta F = -1$ around $(\omega_{if} - \omega_0)/2\pi \sim -1300$ MHz, as well as those with $\Delta F = 1$ around 1300 MHz (not shown on the plot) are suppressed by approximately three orders of magnitude. The "strong" components with $\Delta F = 0$ are spread over an interval of 200 MHz width around the center of the hyperfine structure manifold.

is large, the spectrum is independent of the polarization state of the driving laser field, as expressed by Eq. (24). Very-high (sub-MHz) resolution spectroscopy of MHI could further distinguish the individual Zeeman-split components of the $E2$ transition lines. In that case, the polarization state of the driving laser field becomes relevant, through the factor $\mathcal{W}^{\rm pol}$. Each hyperfine transition line $((vL)FJ) \to ((v'L')F'J')$ is split into a large number of components $((vL)FJJ_z) \to ((v'L')F'J'J'_z)$. The Zeeman structure of one $E2$ transition line is illustrated

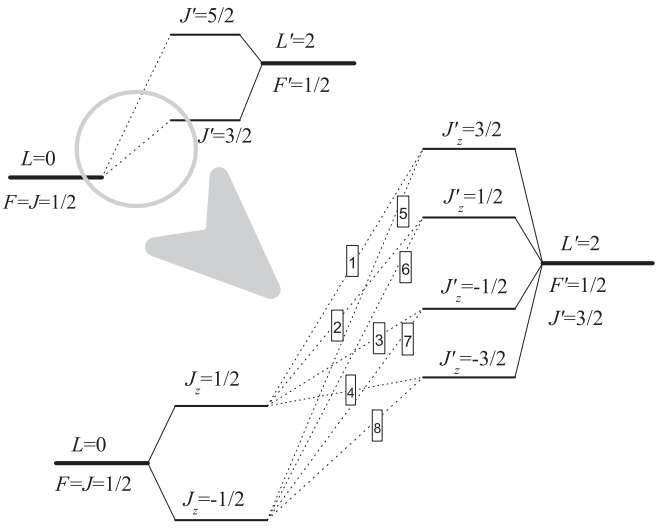

FIG. 2. Zeeman structure of a $(v, L = 0) \to (v', L' = 2)$ transition line of H_2^+. In the presence of external magnetic field the $(F = J = 1/2) \to (F' = 1/2, J' = 3/2)$ hyperfine transition line (circled in the upper panel) is split into eight Zeeman components (lower panel) whose intensities, according to Eqs.(18) and (23), depend strongly on geometry and on the polarization of the laser radiation. For details, see also Table IV.

TABLE III. Hyperfine shifts $\Delta E^{\rm hfs} = E^{\rm hfs}_{(v'L')FJ'} - E^{\rm hfs}_{(vL)FJ}$, in MHz, and relative intensities $\mathcal{W}^{\rm hfs}(FJ';FJ)$ of the "strong" components $(F' = F)$ in the hyperfine spectrum of selected $E2$ transitions in H_2^+. The transitions marked in bold have been identified in Refs. [3,4] as being of particular interest in precision spectroscopy.

F	J	J'	$\Delta E^{\rm hfs}$ (MHz)	$\mathcal{W}^{\rm hfs}(FJ';FJ)$
		$(vL) = (00) \to (v'L') = (12)$		
1/2	1/2	3/2	−59.35740	0.400000
1/2	**1/2**	**5/2**	**39.57160**	**0.600000**
		$(vL) = (01) \to (v'L') = (11)$		
3/2	3/2	1/2	−103.95790	0.011052
3/2	5/2	1/2	−96.11068	0.099861
3/2	3/2	5/2	−20.69538	0.139966
3/2	**3/2**	**3/2**	**−13.42782**	**0.071036**
3/2	**5/2**	**5/2**	**−12.84816**	**0.093333**
3/2	1/2	1/2	−7.40299	0.000000
3/2	5/2	3/2	−5.58060	0.139968
1/2	1/2	3/2	4.97277	0.110877
1/2	1/2	1/2	23.50717	0.000000
1/2	**3/2**	**3/2**	**24.64797**	**0.111017**
1/2	3/2	1/2	43.18237	0.110888
3/2	1/2	5/2	75.85953	0.099849
3/2	1/2	3/2	83.12709	0.011051
		$(vL) = (02) \to (v'L') = (12)$		
1/2	5/2	3/2	−101.51990	0.120000
1/2	**5/2**	**5/2**	**−2.59090**	**0.480000**
1/2	**3/2**	**3/2**	**3.88635**	**0.280000**
1/2	3/2	5/2	102.81535	0.120000
		$(vL) = (03) \to (v'L') = (13)$		
3/2	7/2	3/2	−152.60051	0.005433
3/2	9/2	5/2	−93.57469	0.004237
3/2	5/2	3/2	−86.70920	0.043913
3/2	7/2	5/2	−75.84373	0.057349
3/2	9/2	7/2	−31.67871	0.051879
1/2	5/2	7/2	−21.08081	0.020469
3/2	9/2	9/2	−14.87429	0.181878
3/2	7/2	7/2	−13.94774	0.075715
3/2	5/2	5/2	−9.95241	0.037264
3/2	3/2	3/2	−4.62881	0.045714
3/2	7/2	9/2	2.85668	0.051873
1/2	5/2	5/2	22.61118	0.122044
1/2	7/2	7/2	25.36093	0.169874
3/2	5/2	7/2	51.94357	0.057341
3/2	5/2	9/2	68.74799	0.004235
1/2	7/2	5/2	69.05292	0.020471
3/2	3/2	5/2	72.12798	0.043926
3/2	3/2	7/2	134.02396	0.005433

in Fig. 2, and further details are given in Table IV. The small number of hyperfine and Zeeman components of $E2$ transitions from or to $L = 0$ states makes them particularly appropriate for precision spectroscopy. The linear and quadratic Zeeman shifts have been calculated precisely [3]. For one pair of Zeeman components, $(J = 1/2, J_z = 1/2 \to J' = 5/2, J'_z = \pm 5/2)$ (first bold line in Table III), the Zeeman shifts are smaller than ± 0.2 kHz in a 10 μT field.

The relative intensities of the Zeeman components are described by the factor $\mathcal{W}^{\rm pol}(J_z, J'_z)$ in Eqs. (18) and (23) and strongly depend on geometry and the polarization of the inci-

TABLE IV. Relative intensities $\mathcal{W}^{\rm pol}(J_z,J_z')$ of the Zeeman components of the $(v,L=0,F=J=1/2)\rightarrow(v',L'=2,F'=1/2,J'=3/2)$ hyperfine transition, labeled with the index $n=1,\ldots,8$, as in Fig. 2, for linear and circular polarization of the incident light and a set of angles β between the directions of the laser beam and the magnetic field. The values of $\mathcal{W}^{\rm pol}(J_z,J_z')$ were calculated from Eq. (23), using expressions (26) and (27) for the explicit dependence on the angle β. Note that the relative intensities depend only on the quantum numbers J, J_z, J', and J_z', and are independent of v, v', L, and L', the transition energy, or the magnitude of the Zeeman shift.

			$\mathcal{W}^{\rm pol}(J_z,J_z')$							
			Linear polarization				Left circular polarization			
n	J_z	J_z'	$\beta=0$	$\pi/4$	$\pi/3$	$\pi/2$	0	$\pi/4$	$\pi/3$	$\pi/2$
1	1/2	3/2	0.1250	0.0	0.0312	0.1250	0.0	0.0312	0.0625	0.0625
2	1/2	1/2	0.0	0.3750	0.2813	0.0	0.0	0.1875	0.1406	0.0
3	1/2	−1/2	0.3750	0.0	0.0938	0.3750	0.7500	0.0938	0.0	0.1875
4	1/2	−3/2	0.0	0.1250	0.0938	0.0	0.0	0.3643	0.4218	0.2500
5	−1/2	3/2	0.0	0.1250	0.0938	0.0	0.0	0.0107	0.0469	0.2500
6	−1/2	1/2	0.3750	0.0	0.0938	0.3750	0.0	0.0938	0.1875	0.1875
7	−1/2	−1/2	0.0	0.3750	0.2813	0.0	0.0	0.1875	0.1406	0.0
8	−1/2	−3/2	0.1250	0.0	0.0312	0.1250	0.2500	0.0313	0.0	0.0625

dent electromagnetic radiation. To investigate this dependence we parametrize the complex unit vector $\hat{\epsilon}=\mathbf{E}_0/|\mathbf{E}_0|$ pointing along the electric field amplitude $\mathbf{E}_0$ in the following way. We denote by K the laboratory reference frame with z axis along the external magnetic field $\mathbf{B}$, by K' a reference frame with z axis along $\hat{\mathbf{k}}$, and take the Cartesian coordinates $(\epsilon_x',\epsilon_y',\epsilon_z')$ of ϵ in K' to be $(\cos\theta,\sin\theta\, e^{i\varphi},0)$. Linear polarization of the incident light is described by $\varphi=0$, circular polarization by $\varphi=\pm\pi/2,\theta=\pi/4$, and all other combinations correspond to a general elliptic polarization. Let (α,β,γ) be the Euler angles of the rotation that transform K into K', and denote by $M(\alpha,\beta,\gamma)$ the matrix relating the Cartesian coordinates (a_x,a_y,a_z) and (a_x',a_y',a_z') of an arbitrary vector $\mathbf{a}$ in K and K', respectively: $a_i=\sum_j M_{ij}(\alpha,\beta,\gamma)\,a_j'$. (To avoid mismatch of M with M^{-1}, note that, e.g., $M_{xz}=-\sin\beta\cos\gamma$.) In this way, the absolute values of the components of $\widehat{T}$ in the laboratory frame K, appearing in Eq. (23), are expressed in closed form in terms of the four angles α, β, θ, and φ (the dependence on γ being canceled). Since the general expressions are rather lengthy, we restrict ourselves here to the cases of main interest for the experiment. We have (a) $\varphi=0$ for linear polarization,

$$
\begin{aligned}
|\widehat{T}^{(2)0}|^2 &= \tfrac{1}{4}\sin^2 2\beta\cos^2(\alpha-\theta),\\
|\widehat{T}^{(2)\pm1}|^2 &= \tfrac{1}{12}(1+\sin^2(\alpha-\theta)\cos 2\beta+\cos^2(\alpha-\theta)\cos 4\beta),\\
|\widehat{T}^{(2)\pm2}|^2 &= \tfrac{1}{24}\sin^2\beta\,(3+\cos 2\beta-2\sin^2\beta\cos 2(\alpha-\theta)),
\end{aligned}
\tag{26}
$$

and (b) $\theta=\pi/4,\varphi=\pi/2$ for left circular polarization (l.c.p.),

$$
\begin{aligned}
|\widehat{T}^{(2)\,0}|^2 &= \tfrac{1}{8}\sin^2 2\beta,\\
|\widehat{T}^{(2)\,\pm1}|^2 &= \frac{1}{3}\begin{pmatrix}\sin^4\beta/2\\ \cos^4\beta/2\end{pmatrix}(1\pm 2\cos\beta)^2,\\
|\widehat{T}^{(2)\,\pm2}|^2 &= \frac{1}{3}\begin{pmatrix}\sin^4\beta/2\\ \cos^4\beta/2\end{pmatrix}\sin^2\beta.
\end{aligned}
\tag{27}
$$

For right circular polarization (r.c.p.), described by $\theta=\pi/4$, $\varphi=-\pi/2$, the values of $|\widehat{T}^{(2)q}|^2$ are obtained from the above expressions with the substitution $|\widehat{T}^{(2)q}(\text{r.c.p.})|^2=|\widehat{T}^{(2)-q}(\text{l.c.p.})|^2$.

It is worth stressing that Eqs. (18)–(23) are valid for arbitrary angle β between the magnetic field and the laser propagation direction.

IV. CONCLUSION

We derived the $E2$ transition spectrum of H_2^+, including a systematic consideration of the transition strength and of the effects of the laser polarization. The matrix elements of the electric quadrupole transition moment, needed for the evaluation of the laser-driven transition rates, have been calculated for a very large number of transitions that cover a wide range of transition frequencies, using the most advanced computational methods. The numerical results agree with the results of Refs. [11,12] wherever comparison is possible.

The results can be used in planning future experiments and in interpreting the spectroscopy data. The most basic application of the results presented here is to estimate the laser intensity necessary to achieve a desired transition rate.

The treatment we have given is applicable to the situations when Doppler broadening is present or absent. When it is present, then the individual hyperfine components and Zeeman components may not be resolved. Several components will contribute to the spectroscopic signal even if the laser radiation is perfectly monochromatic. The formula for the strengths of the individual components given here allows for producing a model of the Doppler-broadened line profile which can be used in fitting the experimental signal. As the spectroscopy of MHIs will develop into the Doppler-free regime (Lamb-Dicke regime), the concept of Rabi frequency will become more relevant. This can also easily be computed with the expressions given here.

The presented approach is applicable for any relative size of the hyperfine coefficients and mixing angles ϕ. Thus, it can also be used for molecules in which the coupling between electron spin and rotation (described by the coefficient c_e) is the strongest, opposite to the case in H_2^+. An important example which is drawing substantial attention in connection with spectroscopy in ion traps is N_2^+ [8,24]. Our treatment here is appropriate for the electronic ground state ($X\,^2\Sigma_g^+$) and generalizes the treatment of Ref. [13].

ACKNOWLEDGMENTS

D.B. and P.D. gratefully acknowledge the support of the Bulgarian National Science Fund under Grant No. FNI 08-17, and of the Bulgarian Academy of Sciences under Grant No. DFNP-17-166. D.B. also acknowledges the support of DAAD Grant No. 91618643. V.I.K. acknowledges support from the Russian Foundation for Basic Research under Grant No. 15-02-01906-a.

[1] V. I. Korobov, J. C. J. Koelemeij, L. Hilico, and J.-Ph. Karr, Phys. Rev. Lett. **116**, 053003 (2016).

[2] D. Bakalov, V. I. Korobov, and S. Schiller, Phys. B: At. Mol. Opt. Phys. **44**, 025003 (2011).

[3] J.-Ph. Karr *et al.*, J. Phys.: Conf. Ser. **723**, 012048 (2016).

[4] S. Schiller, D. Bakalov, and V. I. Korobov, Phys. Rev. Lett. **113**, 023004 (2014).

[5] J. C. J. Koelemeij, B. Roth, A. Wicht, I. Ernsting, and S. Schiller, Phys. Rev. Lett. **98**, 173002 (2007)

[6] J. Biesheuvel, J.-Ph. Karr, L. Hilico, K. S. E. Eikema, W. Ubachs, and J. C. J. Koelemeij, Nat. Commun. **7**, 10385 (2016).

[7] S. Alighanbari, M. G. Hansen, V. I. Korobov, and S. Schiller, Nat. Phys. (to be published) (2018), doi:10.1038/s41567-018-0074-3.

[8] M. Germann, T. Xin, and S. Willitsch, Nat. Phys. **10**, 820 (2014).

[9] D. R. Bates and G. Poots, Proc. Phys. Soc. A **66**, 784 (1953).

[10] A. G. Posen, A. Dalgarno, and J. M. Peek, At. Data Nucl. Data Tables **28**, 265 (1983)

[11] H. O. Pilón and D. Baye, J. Phys. B: At. Mol. Opt. Phys. **45**, 065101 (2012).

[12] J.-Ph. Karr, J. Mol. Spectrosc. **300**, 37 (2014).

[13] S. Schiller, I. Kortunov, M. Hernandez Vera, F. Gianturco, and H. da Silva, Jr., Phys. Rev. A **95**, 043411 (2017)

[14] M. Germann and S. Willitsch, Mol. Phys. **114**, 769 (2016).

[15] C. Cohen-Tannoudji, B. Diu, and F. Laloe, *Quantum Mechanics* (Wiley-Interscience, New York, 2006).

[16] Note that for homonuclear molecules with bosonic nuclei these features are modified; for D_2^+, in particular, the total nuclear spin I is no longer an exact quantum number, and mixing of states with $I = 0$ and $I = 2$ will take place in the expansion, analogous to Eq. (11).

[17] See Supplemental Material at http://link.aps.org/supplemental/10.1103/PhysRevA.97.032505 for a list of the transition energies, the Einstein coefficients A, and the reduced matrix elements for $E2$ transitions in H_2^+ for the states with vibrational and rotational quantum numbers $0 \leqslant v \leqslant 10$ and $1 \leqslant L \leqslant 6$.

[18] V. I. Korobov, L. Hilico, and J.-Ph. Karr, Phys. Rev. A **74**, 040502(R) (2006)

[19] J.-P. Karr, F. Bielsa, A. Douillet, J. Pedregosa Gutierrez, V. I. Korobov, and L. Hilico, Phys. Rev. A **77**, 063410 (2008).

[20] D. James, Appl. Phys. B **66**, 181 (1998).

[21] D. Bakalov and S. Schiller, Appl. Phys. B **116**, 777 (2014).

[22] D. A. Varshalovich, A. N. Moskalev, and V. K. Khersonskii, *Quantum Theory of Angular Momentum* (World Scientific, Singapore, 1980), Vol. 6.

[23] V. I. Korobov, D. Bakalov, and H. J. Monkhorst, Phys. Rev. A **59**, R919(R) (1999).

[24] M. Kajita, G. Gopakumar, M. Abe, M. Hada, and M. Keller, Phys. Rev. A **89**, 032509 (2014).